Azimuthal-order variations of surface-roughness-induced mode splitting and scattering loss in high-Q microdisk resonators

Qing Li, Ali A. Eftekhar, Zhixuan Xia, and Ali Adibi*

School of Electrical and Computer Engineering, Georgia Institute of Technology, 777 Atlantic Drive NW, Atlanta, Georgia 30332, USA

**Corresponding author: adibi@ece.gatech.edu*

Received November 25, 2011; revised February 15, 2012; accepted February 29, 2012; posted March 1, 2012 (Doc. ID 158944); published May 2, 2012

We report an experimental observation of strong variations of quality factor and mode splitting among whispering-gallery modes with the same radial order and different azimuthal orders in a scattering-limited microdisk resonator. A theoretical analysis based on the statistical properties of the surface roughness reveals that mode splittings for different azimuthal orders are uncorrelated, and variations of mode splitting and quality factor among the same radial mode family are possible. Simulation results agree well with the experimental observations. © 2012 Optical Society of America

OCIS codes: 230.3990, 140.3945.

Microdisk resonators are among the key building blocks in integrated photonic circuits. Compact and high-quality-factor (high-Q) microdisk resonators have been demonstrated in silicon-on-insulator (SOI) platforms [1,2]. In such high-index-contrast material systems, the intrinsic Q is mainly limited by scattering loss due to imperfect sidewalls and absorption loss due to unpassivated surface states. Furthermore, the sidewall roughness would lift the degeneracy of two otherwise degenerate whispering-gallery modes [i.e., the clockwise (CW) and counterclockwise (CCW) modes], resulting in mode splitting in the resonance spectrum [1].

In this letter, we report an experimental observation that in a high-Q silicon microdisk resonator, the mode splitting can exhibit strong variations over the same radial mode family (i.e., resonant modes with the same radial order and different azimuthal orders). We also observe variations in the intrinsic Q of these modes, which are experimentally found to be scattering-loss limited. While the variation in the intrinsic Q has been briefly mentioned in [3], a detailed investigation of the underlying mechanism is still missing. These variations are distinct from the well-understood results for microspheres with the presence of a single scatterer, which show quite uniform splittings and scattering losses for resonant modes with different azimuthal orders [4]. To explain the experimental observations, we develop a theoretical analysis based on the statistical properties of the sidewall roughness. The analysis shows that mode splittings for resonant modes with different azimuthal orders are uncorrelated; therefore, strong variations among a family of modes with the same radial order are possible. From the same analysis, the variation of the corresponding intrinsic Q can also be understood.

The 10 μm radius microdisk resonator studied here is fabricated on an SOI wafer with a 220 nm thick silicon device layer. As shown by the scanning-electron micrograph (SEM) in Fig. 1(a), the microdisk resonator is pulley-coupled to a 450 nm wide bus waveguide with a coupling length of 6 μm [5]. The linear transmission response shown in Fig. 1(b) implies that different radial mode families are excited. To identify them, we track the resonance wavelength dispersion and compare the measured group indices to theoretical values. The black lines shown in the inset of Fig. 1(b) are the simulated group indices for the lowest five radial TE modes (electric field parallel to the microdisk plane) using an in-house microdisk mode solver based on the three-dimensional (3-D) FEM implemented in the Comsol environment. The red and green squares correspond to the measured group indices for the

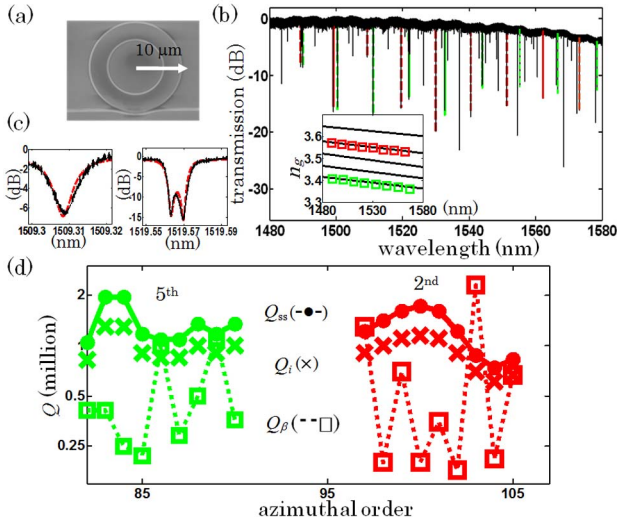

Fig. 1. (Color online) (a) SEM of a 10 μm radius microdisk resonator; (b) transmission of the microdisk resonator at low input power (solid black) and fitting curves for the second-order (dotted red) and fifth-order (dotted green) radial modes; the inset shows the group index comparisons between the finite element method (FEM) simulation (solid black) for the lowest five radial TE modes and the measured ones (with the red and green squares corresponding to the resonances marked by the dotted red and green curves, respectively) from Fig. 1(b); (c) curve-fitting results for the second-order mode around 1509.3 and 1519.6 nm; (d) extracted splitting Q (Q_β, dotted line with squares), intrinsic Q (Q_i, cross), and scattering Q (Q_{ss}, solid line with circles) for the second-order (red, right) and fifth-order (green, left) radial modes, respectively. The vertical axis is shown using the logarithmic scale.

resonances marked by the dotted red and green curves in Fig. 1(b), which are identified to be the second- and fifth-order radial modes, respectively. Based on the mode-splitting model developed in [1], curve fitting is performed to extract the splitting Q (Q_β) and intrinsic Q (Q_i) for these resonances. Two such examples are shown in Fig. 1(c) for two neighboring resonances for the second-order radial mode, with the black curves being the experimental data and the dotted red curves being the fitted data. We show the extracted splitting and intrinsic Q for the second- and fifth-order radial modes in Fig. 1(d), where for each radial mode family strong variations in the splitting Q and milder variations in the intrinsic Q for different azimuthal orders are observed. The variation of the mode splitting is also evident from Fig. 1(c), as for the two neighboring second-order radial modes, one has a strong mode splitting and the other has a negligible mode splitting.

To understand the source of variations of the intrinsic Q among different azimuthal orders, we perform scattering- and absorption-loss measurements. In silicon resonators, when the input power is not too high to generate a significant amount of free carriers, two-photon absorption (TPA) prevails other nonlinear processes. This has two implications. First, the intrinsic cavity loss increases linearly with the cavity energy. Second, as the TPA power is converted to heat, the resonance wavelength undergoes a redshift, which can be used to extract the linear absorption as well as the scattering loss contributions [3]. Figure 2(a) shows the transmission scans for the second-order radial mode around 1509.3 nm at different input power levels. The increase of the extinction ratio with the input power indicates the operation in the overcoupled regime. The nonlinear cavity loss, as shown in the inset of Fig. 2(b), has a linear dependence on the cavity energy, confirming that TPA is the dominant nonlinear process. From the resonance wavelength shift, as shown in Fig. 2(b), the linear absorption loss is inferred to be 25% of the total intrinsic loss. Same measurements are repeated for all the resonances shown in Fig. 1(d), and the extracted scattering Q (Q_{ss}) is plotted in Fig. 1(d). Generally, scattering loss contributes more than 70% to the total intrinsic loss, and within the measurement accuracy the variation of the intrinsic Q among the azimuthal orders can be mostly attributed to the variation of the scattering Q, while the linear absorption Q is fairly uniform [3].

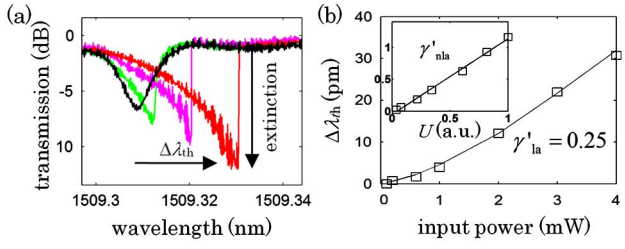

Fig. 2. (Color online) (a) Transmission scans of the second-order radial mode around 1509.3 nm at various input power levels; (b) measured, thermally induced wavelength shift $\Delta\lambda_{th}$ (square) versus the relative input power along with a fit (solid line) for normalized linear absorption γ'_{la} (linear absorption loss normalized to the cold-cavity loss) based on the model in [3]. The inset shows the measured, normalized nonlinear absorption γ'_{nla} (shown by square, which is the nonlinear absorption loss normalized to the cold-cavity loss) versus the relative cavity energy along with a linear fit (solid line). The input power is the power sent from the testing laser, and the circulating power inside the resonator is approximated to be around 50 mW at 1 mW input power in our characterization setup.

To explain the experimental observation that the mode splitting and scattering loss vary over different azimuthal orders, a theoretical analysis is needed. In a straight waveguide, the sidewall roughness $\Delta r(x)$ is characterized by its autocorrelation function, which is usually approximated as

$$\langle \Delta r(x)\Delta r(x')\rangle = \sigma^2 \exp\left(-\frac{|x-x'|^2}{L_c^2}\right), \tag{1}$$

where $\langle\rangle$stands for the ensemble average, x is the direction along the waveguide, σ is the roughness standard deviation, and L_c is the correlation length [1]. In a microdisk, because of the periodic boundary condition, $\Delta r(x)$ can be expanded in terms of periodic harmonics along the disk perimeter as

$$\Delta r(\phi) = \frac{1}{2\pi}\sum_n F(k_n)e^{ik_nR\phi}, \tag{2}$$

$$F(k_n) = \int_0^{2\pi} \Delta r(\phi)e^{-in\phi}\mathrm{d}\phi, \tag{3}$$

where R is the radius of the disk, ϕ is the azimuth, and $F(k_n)$ is the Fourier component of $\Delta r(\phi)$ with $k_n = n/R$ [$n = \pm1, \pm2, \ldots F(k_0) = 0$]. Extending the statistical property imposed by Eq. (1) to microdisk resonators ($x = \phi R$), we obtain

$$\langle F(k_n)F^*(k_m)\rangle = \frac{2\pi^{3/2}(\sigma^2 L_c)}{R} \exp\left[-\left(\frac{k_nL_c}{2}\right)^2\right]\delta(n-m), \tag{4}$$

which shows that the values of $[F(k_n)]$ ($n > 0$) are statistically independent random variables {to ensure $\Delta r(\phi)$ is real, $F(k_{-n}) = [F(k_n)]^*$}. Each resonator is one possible realization of $[F(k_n)]$, and Eq. (4) is valid when the ensemble averaging is performed for many independently fabricated resonators under the same condition. However, Eq. (4) also shows, for one specific resonator, the values of $[F(k_n)]$ are very unlikely to be equal (for different n), and variations among $[F(k_n)]$ are almost certain. As shown by the mode-splitting model in [1], the mode splitting for resonant mode with azimuthal order m is proportional to $|F(k_{2m})|$, which provides the momentum compensation needed to couple the CW and CCW modes. Because of the independence of $[F(k_n)]$ ($n > 0$), different azimuthal modes can exhibit uncorrelated splittings. Strong variation of splitting Q as observed in Fig. 1(d) is thus possible if $[F(k_n)]$ ($n > 0$) values have large amplitude fluctuations.

The scattering loss is calculated using the volume current method [1]. Using the exact form of $\Delta r(\phi)$ in Eq. (1), we obtain the far-field vector potential A as

$$A_{z,m}(r,\theta,\phi) = C_0E_{z,m}(R,0)\sum_n F^*(k_{m+n})(ie^{i\phi})^{-n} \times J_n[k_0R\sin(\theta)], \tag{5}$$

$$A_{\phi,m}(r,\theta,\phi) = \frac{1}{2} C_0 E_{\phi,m}(R,0) \times \sum_n F^*(k_{n+m}) i (ie^{i\phi})^{-n} \times \{J_{n-1}[k_0 R \sin(\theta)] - J_{n+1}[k_0 R \sin(\theta)]\}, \quad (6)$$

with

$$C_0 = \frac{-i\omega h \delta n^2 R}{4\pi c^2} \left(\frac{e^{-ik_0 r}}{r}\right), \quad (7)$$

where $E_{z,m}(R,0)$ $[E_{\phi m}(R,0)]$ is the unperturbed dominant electric field of the azimuthal order m at the disk edge for TM (TE) polarization; $i = \sqrt{-1}$; h is the disk slab thickness; ω is the optical frequency; δn^2 is the refractive index perturbation due to the scattering center; c is the speed of light in vacuum; k_0 is the wave vector in the surrounding medium; and $J_n(x)$ is the Bessel function of the first kind of order n of x. The coordinate variables r, θ, ϕ, and z are graphically defined in Fig. 3(a). Note that in Eqs. (5) and (6) the contribution of $F(k_{m+n})$ is weighed by $J_n(x)$, whose value is only significant when $|n| < |x|$. As a result, only a limited number of $F(k_{m+n})$ effectively contribute to the scattering loss ($|n| < k_0 R$). This is the so-called phase-matched radiation [6]. The limited sum of $[F(k_n)]$ in Eqs. (5) and (6) cannot average out the variation among $[F(k_n)]$, resulting in variations of the scattering loss for different azimuthal orders.

To verify the above qualitative discussion, we model $[F(k_n)]$ by assuming a Gaussian distribution for its amplitude and uniform distribution for its phase as

$$F(k_n) = \sqrt{\frac{2\pi^{3/2}(\sigma^2 L_c)}{R} \exp\left[-\left(\frac{k_n L_c}{2}\right)^2\right]} \times [\cos(\alpha) + \sin(\alpha) N_n(0,1)] \exp[2\pi i U_n(0,1)] \quad (n > 0), \quad (8)$$

where $[N_n(0,1)]$ are independent random variables with a normal distribution with a zero mean and a unit variance and $[U_n(0,1)]$ are independent random variables with a uniform distribution in the interval (0, 1). The parameter α is introduced to account for the amplitude variations of $[F(k_n)]$. The independent uniformly distributed phase terms $\exp[2\pi i U_n(0,1)]$ will ensure the independence of $[F(k_n)]$, as required by Eq. (4). Substituting $[F(k_n)]$ into Eq. (2), the splitting Q can be obtained from the mode-splitting model developed in [1]. The scattering Q, on the other hand, can be calculated from Eq. (6) following the straightforward radiation-loss computation. The electric field $E_{\phi m}(R,0)$ is evaluated from the 3-D FEM simulations, followed by a subsequent averaging along the vertical dimension of the slab. The FEM simulations show that, for the first few order radial modes, the normalized electric fields at the sidewall are almost the same. Therefore, the radial mode order will not be distinguished in the following simulation example. The surface roughness parameters σ and L_c and the amplitude variation parameter α are fitted to generate close results to the experimental data. The simulation results are shown in Fig. 3(b), with $\sigma = 2$ nm, $L_c = 160$ nm, and $\alpha = 0.5\pi$. Figure 3(c) plots the autocorrelation function of the surface roughness with these parameters. Comparing Fig. 3(b) with Fig. 1(d), similar variational patterns in both splitting Q and scattering Q are observed. Note that because of the random nature of $[F(k_n)]$, as illustrated by Eq. (8), Fig. 3(b) is just one possible result. Different simulation runs will generate similar but not exactly the same outcomes. This in fact closely mimics the real fabrication, which produces resonators with comparable but rarely identical performances. In Fig. 3(b), we have also plotted the case with $\alpha = 0$ and the random phase term in Eq. (8) removed (with other parameters being the same). This corresponds to the example mentioned at the beginning, namely, a microsphere with a single scatterer, where $[F(k_n)]$ values are strongly correlated in phase and amplitude {$[F(k_n)]$ are equal in this case}. The resultant mode splitting and scattering loss are fairly uniform, as expected.

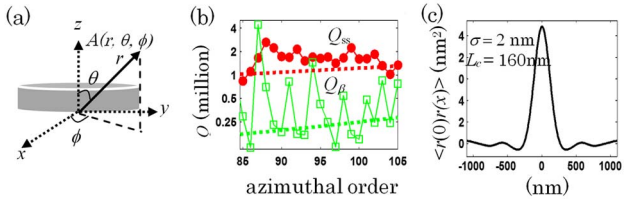

Fig. 3. (Color online) (a) Schematic of the volume current method for scattering loss calculation; (b) simulated scattering Q (solid red line with circles) and splitting Q (solid green line with squares) for $\alpha = 0.5\pi$ in Eq. (8). The red and green dotted lines correspond to the scattering and splitting Q, respectively, for the case with $\alpha = 0$ and no phase variation in Eq. (8). The vertical axis is shown using the logarithmic scale. (c) The autocorrelation function of the sidewall roughness with parameters used in (b).

In conclusion, we have experimentally observed and theoretically explained the variations of mode splitting and scattering loss among the same radial mode family of a high-Q microdisk resonator. Unlike the single-scatterer case, the randomly distributed multiple scatterers present in the microdisk sidewall follow a stationary statistic, which leads to independent mode splittings and variations in the scattering loss. This result is important for the fundamental understanding of the high-Q microdisk resonators as well as for many applications. For example, it explains the fact that in practice the very high Q value is observed only for one particular azimuthal order, while Q of the rest of modes in the same radial mode family can be more than 30% less [2]. When working with multiple azimuthal orders such as four-wave mixing, the designer should be aware of such variations to avoid unexpected results.

This work was supported by the Defense Advanced Research Projects Agency (DARPA) Microsystems Technology Office (MTO) under grant No. 2106ATG.

References

1. M. Borselli, T. J. Johnson, and O. Painter, Opt. Express **13**, 1515 (2005).
2. M. Soltani, S. Yegnanarayanan, and A. Adibi, Opt. Express **15**, 4694 (2007).
3. M. Borselli, T. J. Johnson, and O. Painter, Opt. Lett. **32**, 2954 (2007).
4. D. S. Weiss, V. Sandoghdar, J. Hare, V. Lefevre-Seguin, J. M. Raimond, and S. Haroche, Opt. Lett. **20**, 1835 (1995).
5. Q. Li, M. Soltani, S. Yegnanarayanan, and A. Adibi, Opt. Express **17**, 2247 (2009).
6. B. E. Little and S. T. Chu, Opt. Lett. **21**, 1390 (1996).